

The derivative of the Kardar-Parisi-Zhang equation is not in the KPZ universality class

Enrique Rodríguez-Fernández^{1,*} and Rodolfo Cuerno^{1,†}

¹*Departamento de Matemáticas and Grupo Interdisciplinar de Sistemas Complejos (GISC)
Universidad Carlos III de Madrid, Avenida de la Universidad 30, 28911 Leganés, Spain*

The Kardar-Parisi-Zhang (KPZ) equation is a paradigmatic model of nonequilibrium low-dimensional systems with spatiotemporal scale invariance, recently highlighting universal behavior in fluctuation statistics. Its space derivative, namely the noisy Burgers equation, has played a very important role in its study, predating the formulation of the KPZ equation proper, and being frequently held as an equivalent system. We show that, while differences in the scaling exponents for the two equations are indeed due to a mere space derivative, the fluctuations behave in a remarkably different way: while KPZ displays Tracy-Widom statistics, its derivative displays Gaussian behavior, hence being in a different universality class. We reach this conclusion via direct numerical simulations of the equations, supported by a dynamic renormalization group analysis of field statistics.

The Kardar-Parisi-Zhang (KPZ) equation [1] describes the space-time evolution of a scalar field $h(\mathbf{r}, t)$ as

$$\partial_t h = \nu \nabla^2 h + (\lambda/2)(\nabla h)^2 + \eta, \quad (1)$$

$$\langle \eta(\mathbf{r}, t) \eta(\mathbf{r}', t') \rangle = 2D \delta(\mathbf{r} - \mathbf{r}') \delta(t - t'), \quad (2)$$

where $\mathbf{r} \in \mathbb{R}^d$; $\nu, D > 0$, and λ are parameters, and η is zero-average, Gaussian white noise. This continuum model is a landmark of current Statistical Physics [2, 3], being considered even on a par with the Ising model [4]. Indeed, 24 years and mathematical *tours de force* were required for nontrivial exact solutions to be achieved in the cases of both, the Ising model [5] and the KPZ equation [6–8]. The former (latter) model constitutes a paramount universality class for equilibrium (non-equilibrium) critical phenomena, defined by universal behavior of critical exponents, correlation functions, and amplitude ratios [9, 10]. The KPZ equation in particular, having been originally proposed to model interface growth [1], displays critical behavior which is currently being identified in widely disparate contexts, including bacterial populations [11], turbulent liquid crystals [12], non-linear oscillators [13], stochastic hydrodynamics [14], colloidal aggregation [15], thin film deposition [16, 17], reaction-diffusion systems [18], random geometry [19], superfluidity [20], active matter [21], or quantum entanglement [22].

While, from the point of view of exact integrability, the Ising model is most theoretically fertile in two-dimensions (2D) [9], for KPZ this happens for $d = 1$. Here, fluctuation statistics have been proven to be described, depending on global constraints on system size L and/or initial conditions, by some member of the Tracy-Widom (TW) family of probability distribution functions (PDF) for the largest eigenvalue of random matrices [10, 23], demonstrating KPZ behavior as a conspicuous instance among systems with non-Gaussian fluctuations [24]. Now the universality class incorporates the field statistics, the precise flavor of the TW distribution leading to universality sub-classes in the KPZ case [10, 23].

Historically, a major role in delineating KPZ universality has been played by the stochastic or noisy Burgers equation,

$$\partial_t u = \nu \partial_x^2 u + \lambda u \partial_x u + \partial_x \eta, \quad (3)$$

where η is as in Eq. (2). Clearly, the space derivative of Eq. (1) yields Eq. (3) if $u = \partial_x h$. This relation was exploited

e.g. in [1] to seminally obtain the exact scaling exponents by adapting the earlier dynamical renormalization group (DRG) analysis [25] of Eq. (3), as a model of a randomly stirred fluid. The noisy Burgers equation [26–28] is a paramount system on its own, e.g. for fluid [29] and plasma [30] turbulence, or for interacting particle [31] and driven-diffusive systems [2].

Actually, both 1D equations, (1) [3, 32, 33] and (3) [31], share an “accidental” fluctuation-dissipation symmetry by which the nonlinear term does not influence the corresponding stationary solution of the Fokker-Planck equation governing the field PDF, \mathcal{P} , which becomes a Gaussian, equilibrium-like distribution, determined by the linear and the noise terms [3, 31, 33]. Combined with the shared symmetry under Galilean transformations, this allows to show that the two equations share the non-trivial $z = 3/2$ value for the dynamic exponent describing the power-law increase of the correlation length, $\xi(t) \sim t^{1/z}$ [32, 33]. The roughness exponent α that quantifies the scaling of the field root-mean-square deviation with system size at saturation [32, 33], $w_2 \sim L^\alpha$, differs as expected ($\alpha_{\text{KPZ}} = \alpha_{\text{Burgers}} + 1 = 1/2$), since $h(x) = \int_{x_0}^x u(x') dx'$. Thus, Eqs. (1) and (3) are frequently considered as two equivalent descriptions of a same underlying process. However, the KPZ equation shows that Gaussian behavior for the stationary \mathcal{P} does *not* imply that the height statistics prior to saturation (for $L < \infty$) are also Gaussian; indeed, they are TW-distributed for KPZ [10, 23].

From the point of view of the specific physical systems which are described by the noisy Burgers equation [2, 29–31], it is crucial to clarify whether their fluctuation statistics are also non-Gaussian in the growth regime, in order to accurately identify the universality class of their kinetic roughening behavior. In this Letter we show that this is not the case, i.e., we show that the one-point PDF for $u(x, t)$ as described by Eq. (3) is Gaussian for times dominated by the non-linearity, crucially prior-to and (as expected) after saturation to steady state. We reach this conclusion by direct numerical simulations of the equation, which are analytically supported by a DRG analysis of the field statistics for Eq. (3). In particular, we also address the dynamics of the space-integral of Eq. (3), explicitly illustrating that, in this case, the KPZ sum, $h(x, t)$, of (correlated) Gaussian Burgers variables $u(x, t)$ indeed yields TW-distributed fluctuations.

We begin by addressing the full time dynamics described by Eq. (3). While the invariant measure of the equation has been shown [26, 27, 31] to be Gaussian, and the asymptotic scaling exponents are analytically known via DRG [25, 34], to our knowledge the time crossover which occurs from linear to nonlinear behavior has not been explicitly addressed yet. In order to assess it, we have performed numerical simulations of Eq. (3). Note, this model is known to be conspicuously prone to numerical instabilities [35]. We use the numerical scheme proposed in [36], which provides consistent results. Considering flat initial conditions and periodic boundary conditions, we show in Fig. 4 the time evolution of the structure factor $S(k, t) = \langle \tilde{\phi}(k, t) \tilde{\phi}(-k, t) \rangle$, as described by Eq. (3); here, tilde denotes spatial Fourier transform and k is wave number. Panel (a) corresponds to $\phi(x, t) = u(x, t)$, while panel (b) is for its space integral, $\phi(x, t) = h(x, t) = \int_0^x u(x', t) dx'$, which should retrieve the behavior expected for Eq. (1). At relatively early times, the linear term and the noise in Eq. (3) are expected to control the evolution of both the u and h fields, hence $z = 2$ as provided by the exact solution of the linearized equation [33]. This behavior is approximately reproduced by our simulations, as implied by the data collapse shown in the insets for small times. Indeed, recall that, under kinetic roughening conditions, $S(k, t) \sim k^{-(2\alpha+1)} s(kt^{1/z})$, with $s(u) \sim 1$ for $u \gg 1$ and $s(u) \sim u^{2\alpha+1}$ for $u \ll 1$ [32, 33]. Collapse is achieved for u (h) using $\alpha = -1/2$ ($1/2$), as also borne out from the exact solution of the linearized equations (3) and (1), respectively. However, for sufficiently long times, the value of z changes, indicating nonlinear behavior. Indeed, data collapse is now obtained using $z = 3/2$ both, for u and for h , as expected in the asymptotic limit [1, 25]. Note that, also in both cases, α remains fixed to its linear-regime value as a consequence of the ‘‘accidental’’ fluctuation-dissipation symmetry [3, 31–33]. Overall, Eq. (3) is thus seen to account for the full dynamics of the Burgers field, and for the KPZ behavior of its space integral. Conversely, in the Appendix I we integrate numerically the KPZ equation (1) showing that the evolution of its slope field $u(x, t) = \partial_x h(x, t)$ coincides with results from Eq. (3). All this supports, as expected, the identification of the solutions of Eq. (3) with the slopes of the solutions of the KPZ equation.

Beyond scaling exponents, we have also studied numerically the field fluctuations described by Eq. (3), defined as

$$X(x, \Delta t, t_0) = (\Delta\phi - \overline{\Delta\phi}) / (\Gamma \Delta t)^\beta, \quad (4)$$

where $\Delta\phi(x, \Delta t, t_0) = \phi(x, t_0 + \Delta t) - \phi(x, t_0)$, bar denotes space average, $\beta = \alpha/z$ is the growth scaling exponent, Γ is a normalization constant [37], and $\Delta t \gg 1$ will be assumed. In principle, the statistical distribution of the fluctuations can differ before ($t_0 = 0, \Delta t \ll t_{sat}$) and after ($t_0 > t_{sat}$) saturation. E.g., for a periodic KPZ system, they are provided by the TW distribution for the largest eigenvalue of random matrices in the Gaussian Orthogonal Ensemble (TW-GOE) and by the Baik-Reins (BR) distributions, respectively [10, 23, 37].

We assess in Fig. 5 the fluctuations of the u and h fields, as numerically obtained from Eq. (3). Full PDFs are shown

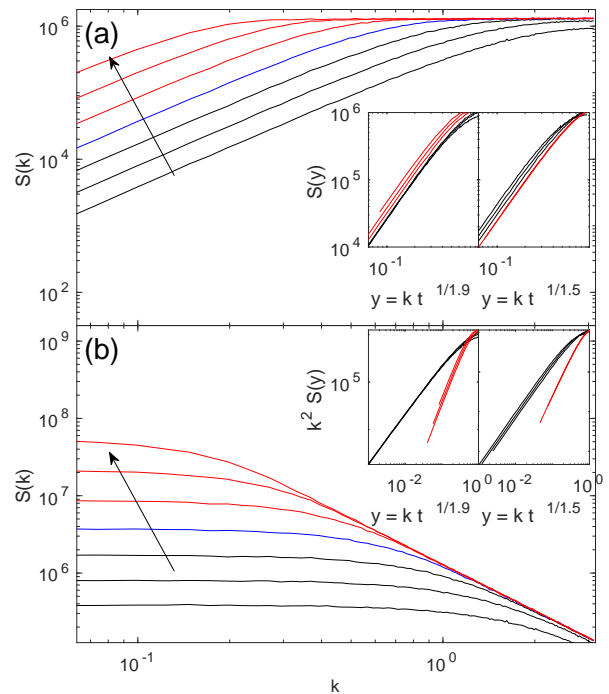


FIG. 1: Time evolution of the structure factor described by Eq. (3) for (a) $u(x, t)$ and (b) $h(x, t) = \int_0^x u(x', t) dx'$, using $D = \nu = 1$, $\lambda = 4$, and $L = 256$. Black (red) solid lines correspond to the linear (nonlinear) regime, as implied by the data collapses in the insets. The arrows indicate time increase, t for each line being twice that of the previous one, starting at $t_0 = 0.64$. All units are arbitrary.

in Figs. 5(a) and 5(b) for times both in the nonlinear growth regime determined above ($t_0 + \Delta t < t_{sat}$) and after saturation to steady state ($t_0 > t_{sat}$). Figures 5(c) and 5(d) show the corresponding time evolution of the field skewness, $\mathcal{S} = \langle X^3 \rangle_c / \langle X^2 \rangle_c^{3/2}$ and excess kurtosis, $\mathcal{K} = \langle X^4 \rangle_c / \langle X^2 \rangle_c^2$, respectively, where $\langle X^n \rangle_c$ denotes the n -th order cumulant. The statistics of $u(x, t)$ are Gaussian to a high precision, both prior to and after saturation, see the PDFs in panels (a,b). Indeed, the skewness and (somewhat more slowly) the excess kurtosis converge rapidly to zero [panels (c,d)] for $u(x, t)$. The slope field of Eq. (1) exhibits a similar Gaussian behavior, as shown in Fig. 5 in the Appendix I, again in agreement with the identification of the noisy Burgers equation, Eq. (3), as the continuum description of the slopes field for the KPZ equation.

In the case of the $h(x, t)$ field, Eq. (3) correctly leads $\mathcal{S}(t)$ and $\mathcal{K}(t)$ to take on the characteristic universal values of the KPZ equation, either TW-GOE or BR [shown as blue or red solid lines, respectively, in Figs. 5(c) and (d)] for intermediate values of Δt within the expected ranges of t_0 and Δt ($t_0 = 0, t_{sat} > \Delta t \gg 0$ and $t_0 > t_{sat}, t_0 > \Delta t \gg 0$, respectively). Indeed, the PDF of h fluctuations approaches the TW-GOE or BR distributions for $t_0 = 0$ or $t_0 = t_{sat}$, respectively, only for such intermediate values of Δt . This behavior has been also observed for discrete and continuum models in the KPZ universality class [37, 38]. Specifically, the difference

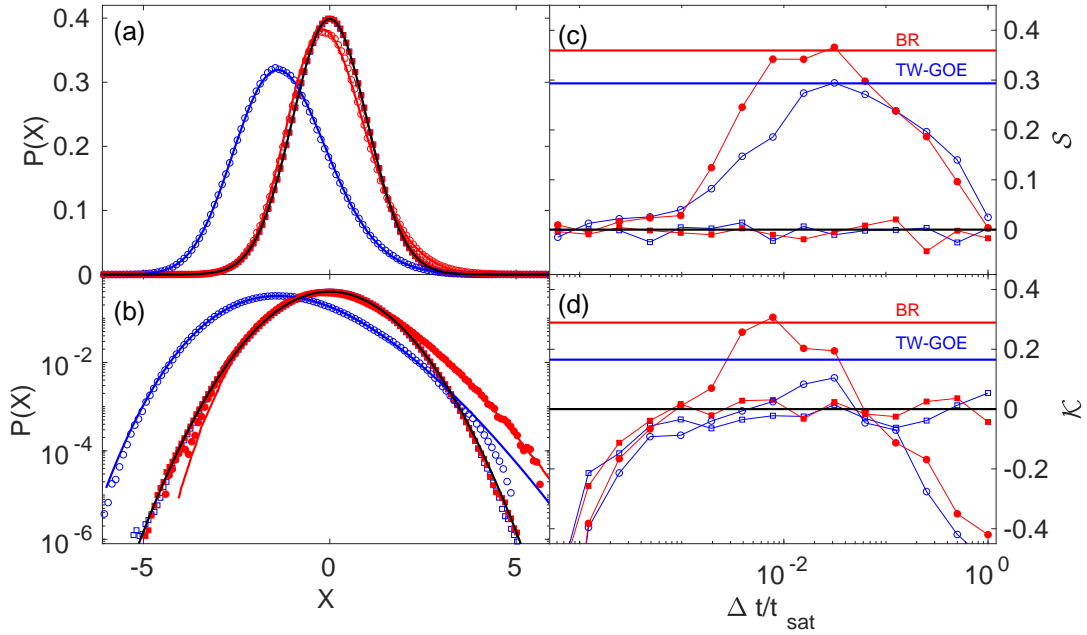


FIG. 2: Fluctuation histogram (a,b) from simulations of Eq. (3) with $\nu = 1$, $\lambda = 10^3$, $D = 10^{-3}$, and $L = 256$, for $\phi = u$ (squares) and $\phi = h(x, t) = \int_0^x u(x', t) dx'$ (circles). Means and variances have been adjusted to TW-GOE and BR values. Dynamics of skewness (kurtosis) appears in (c) [(d)]. In all panels blue (red) and empty (filled) symbols correspond to the growth (saturation) regime, with black, blue, and red solid lines showing exact Gaussian, TW-GOE, and BR values, respectively; $t_{\text{sat}} = 100$, and $\Delta t = 25 - 50$, $1.5 - 3$, and $0.4 - 0.8$ are used for Gaussian, TW-GOE, and BR-like histograms, respectively. Thin lines in (c,d) are guides to the eye. All units are arbitrary.

between the actual PDF and the ideal TW-GOE or BR distributions reaches a minimum for intermediate values of Δt . It is for such Δt that the numerical h -PDF is plotted in Figs. 5(a,b). Means and variances have been adjusted to equal those of the exact TW-GOE or BR distributions. As the pre- or post-saturation h -PDF evolves from Gaussian to TW-GOE or BR, to become Gaussian again for large Δt [see panels 5(c,d)], the Gaussian black solid line on panels 5(a,b) seems to attract the tails of the h distribution.

The Gaussian behavior obtained for u as described by Eq. (3) coincides with analytical expectations derived from a DRG evaluation of the field cumulants, which is described next. We take an approach which has been successfully employed for the KPZ [39–41] and nonlinear-Molecular Beam Epitaxy (MBE) [42] equations, and for the scalar Burgers equation with *non*-conserved noise [43]. The method performs a partial RG transformation only, in which a coarse-graining of the equation is performed, while omitting the standard additional rescaling step [25, 34]. This allows to make explicit the scale-dependence of the equation parameters, as seminally proposed in [44]. Under this DRG approach, the n -th cumulant reads,

$$\langle u^n \rangle_c = \int_{\mathbb{R}^{2(n-1)}} G(k_n, \omega_n) L_n \prod_{j=1}^{n-1} \frac{dk_j d\omega_j}{(2\pi)^2} G(k_j, \omega_j), \quad (5)$$

where $k_n = -\sum_{j=1}^{n-1} k_j$, $\omega_n = -\sum_{j=1}^{n-1} \omega_j$, and L_n are correction factors to be evaluated perturbatively. Within a one-

loop approximation [39–43] (see Appendix II for details),

$$\begin{aligned} \langle u^n \rangle_c &= A \int_{\mathbb{R}^{2(n-1)}} G(k_n, \omega_n) k_n \\ &\times \prod_{i=1}^{n-1} \frac{dk_i d\omega_i}{(2\pi)^2} k_i G(k_i, \omega_i) k_i^{3/2} \nu^2(k_i) |G(k_i, \omega_i)|^2, \end{aligned} \quad (6)$$

where $A = \pi^{n-1/2} i^n \Gamma(n-1/2) 2D(2n-2)!! / [n!(n-1)\lambda^{n-2}]$. Integration of Eq. (19) for $n = 2$ yields the variance,

$$\begin{aligned} w_2^2 = \langle u^2 \rangle_c &= A \int_{\mathbb{R}^2} \frac{dk_1 d\omega_1}{(2\pi)^2} k_1^{7/2} \nu^2(k_1) |G(k_1, \omega_1)|^4 \\ &= B \int_{\mathbb{R}} dk_1, \end{aligned} \quad (7)$$

where B is a numerical constant. Considering non-zero, finite lattice spacing, s , and system size, L , the variance of u scales as $1/L$, which indeed agrees with the expected value of the roughness exponent, $\alpha = -1/2$. Moreover, the variance diverges as $w_2^2 \sim s^{-1}$ for $s \ll 1$ [33]. We have additionally characterized the divergence of the fourth cumulant, $\langle u^4 \rangle_c$, with lattice spacing to determine the asymptotic behavior of the kurtosis, $\mathcal{K} = \langle u^4 \rangle_c / \langle u^2 \rangle_c^2$. We obtain (see Appendix III) $\langle u^4 \rangle_c \sim [\ln(1/s)]^{0.79}$ leading to a vanishing field kurtosis in the $s \rightarrow 0$ limit. This result is consistent with our numerical simulations, which show Gaussian statistics for the field u . Such a conclusion is strengthened by the values taken by arbitrary odd-order cumulants (odd n). Again considering

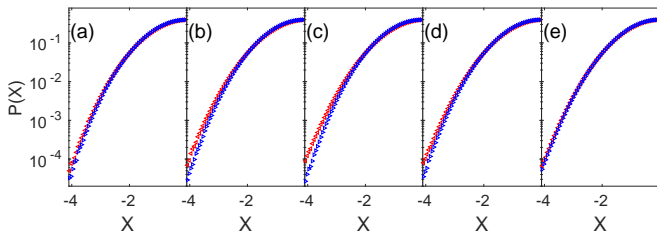


FIG. 3: Fluctuation histogram for the slope field $\phi = \partial_x u$ [with $X = (\phi - \bar{\phi})/\text{std}(\phi)$] from numerical simulations of Eq. (3), using $\nu = 1$, $\lambda = 10^4$, $D = 10^{-3}$, and $L = 256$, for times in the linear (a), nonlinear (b), (c), (d), and saturation (e) regimes [time for each panel is twice that of the previous one, starting at $t_0 = 40$ (a)]. The $X > 0$ data (red left triangles) have been reflected to facilitate comparison with $X < 0$ data (blue right triangles). All units are arbitrary.

Eq. (19), after integration in $\{\omega_i\}_{i=1}^{n-1}$ the integrand becomes $k_n g(k_1, \dots, k_n) \prod_{i=1}^{n-1} k_i$, where all k_i in $g(\cdot)$ are to be taken in absolute value. As shown in [43], this fact leads to an exact cancellation of the additional integral in the $\{k_i\}_{i=1}^{n-1}$ variables for arbitrary odd values of n . Hence, the u -PDF is necessarily symmetric (as a Gaussian, but unlike the TW or BR distributions), as all its odd cumulants are zero [43].

Our numerical and analytical results hence indicate that the long-time behavior of Burgers equation with conserved noise, Eq. (3), albeit being controlled by the nonlinear term, displays Gaussian fluctuations. This is in spite of the fact that it is precisely such nonlinearity which breaks the inversion symmetry ($u \leftrightarrow -u$) of the equation. This lack of symmetry is correlated in the KPZ context [33] with a non-zero skewness due to the existence of a preferred growth direction, as likewise occurs for the nonlinear-MBE equation [45]. Hence, the symmetry of the (Gaussian) PDF is an emergent property of the large-scale behavior in Eq. (3), much like it is for Burgers equation with *non-conserved* noise [43]. Akin to the latter, the symmetric fluctuations in the nonlinear regime can be related with the behavior of the deterministic (viscous) Burgers equation, which is analytically known [46, 47] to yield sawtooth profiles, symmetric around their mean and, as Eq. (3) itself, under a combined $(x, u) \leftrightarrow (-x, -u)$ transformation. Such an action by the nonlinear term in Eq. (3) can be specifically assessed in the slopes histogram, again similar to Burgers equation with non-conserved noise [43, 48], becoming naturally enhanced for large λ and small ν and D values. Figure 3 shows the time evolution of the PDF of slope ($\partial_x u$) fluctuations, which indeed evolves from a symmetric form in the early linear regime to a non-symmetric form in the nonlinear regime, to finally become symmetric again at saturation. Once again, similar behavior is observed in numerical simulations of the KPZ equation, Eq. (1), now for the *curvatures* ($\partial_x^2 h$) of the KPZ profiles, see Fig. 6 in Appendix I.

Finally, let us remark that the Gaussian nature of the fluctuations displayed by Eq. (3) in its large-scale nonlinear regime allows for an exact Gaussian (asymptotic) approximation of the equation. Namely, a *linear* model in the same univer-

sality class, including scaling exponent values *and* Gaussian fluctuation statistics, can be readily formulated. Again, this is akin to the case of the scalar Burgers equation with non-conserved noise [43], including higher-dimensional and strongly anisotropic generalizations [49, 50], as the celebrated Hwa-Kardar equation for the height of a running sandpile [51]. In contrast with these, Eq. (3) does *not* support the hyperscaling relation ($2\alpha + d = z$) [32, 33], hence spatial correlations in the noise are required in order to match the full universal behavior. Specifically, the linear, non-local equation

$$\partial_t \tilde{u}(k, t) = -|k|^{3/2} \tilde{u}(k, t) + \tilde{\eta}(k, t), \quad (8)$$

$$\langle \tilde{\eta}(k, t) \tilde{\eta}(k', t') \rangle = |k|^{3/2} \delta(k + k') \delta(t - t'), \quad (9)$$

yields the exact same asymptotic behavior of the nonlinear Eq. (3). Note that a similar exact Gaussian approximation is not possible for systems with non-Gaussian statistics (like the KPZ equation), not even considering correlations in the noise.

In summary, we have obtained that the field fluctuations of the Burgers equation with conserved noise are Gaussian-distributed, in spite of the facts that its asymptotic behavior is controlled by a nonlinear term which explicitly breaks the up-down symmetry and that the equation is related to the KPZ equation through a mere space derivative, statistics becoming paradigmatically non-Gaussian. Such non-symmetric fluctuation behavior indeed occurs both, for the integral and the slope fields related with the u field described by Eq. (3), as manifested by Figs. 5 and 3, respectively. In particular, all this behavior provides an explicit, nontrivial example in which the KPZ sum, $h(x, t) = \int_{x_0}^x u(x', t) dx'$, of (correlated) Gaussian Burgers variables $u(x, t)$ yields TW-distributed fluctuations. The correct identification of the universality class (including scaling exponent values and class of fluctuation statistics) is paramount to fully identify stochastic Burgers behavior in the many contexts of spatially-extended systems, from fluid turbulence to driven diffusive systems, in which Eq. (3) plays a relevant role as a physical model.

We acknowledge valuable comments by M. Castro, J. Krug, and P. Rodriguez-Lopez. This work has been supported by Ministerio de Economía y Competitividad, Agencia Estatal de Investigación, and Fondo Europeo de Desarrollo Regional (Spain and European Union) through grant No. FIS2015-66020-C2-1-P. E. R.-F. also acknowledges financial support by Ministerio de Educación, Cultura y Deporte (Spain) through Formación del Profesorado Universitario scholarship No. FPU16/06304.

APPENDIX I: Noisy Burgers equation as the derivative of the KPZ equation

To further assess the relation between Burgers equation with conserved noise (spell out noisy Burgers equation),

$$\begin{aligned} \partial_t u &= \nu \partial_x^2 u + \lambda u \partial_x u + \partial_x \eta, \\ \langle \eta(x, t) \eta(x', t') \rangle &= 2D \delta(x - x') \delta(t - t'), \end{aligned} \quad (10)$$

and the Kardar-Parisi-Zhang (KPZ) equation,

$$\begin{aligned} \partial_t h &= \nu \partial_x^2 h + (\lambda/2)(\partial_x h)^2 + \eta, \\ \langle \eta(x, t) \eta(x', t') \rangle &= 2D \delta(x - x') \delta(t - t'), \end{aligned}$$

namely, that the former is the space derivative of the latter. We simulate numerically both, Eq. (10) and (11), taking space derivative of the latter for each time and noise realization, and then compute the structure factor for both numerical fields. Recall that the stochastic nonlinear equations we are discussing are conspicuously prone to numerical inaccuracies and instabilities [36], which renders nontrivial the present type of check which we are performing. Results are provided on Fig. 4, in which panel (a) corresponds to Eq. (10) [thus repeating the same data shown on Fig. 1(a) for reader's convenience] and panel (b) corresponds to the numerical derivative of the KPZ profile described by Eq. (11). As expected, results are virtually indistinguishable, hence consistent with the behavior discussed above for the Burgers equation with conserved noise, namely, early-time (linear regime) exponent values $z_{\text{linear}} = 1.9$, $\alpha_{\text{linear}} = -1/2$ and late-time (nonlinear regime) exponent values $z_{\text{nonlinear}} = 3/2$, $\alpha_{\text{nonlinear}} = -1/2$.

We proceed similarly to compute the probability distribution function (PDF) of field fluctuations [as defined in Eq. (4)] both, for Eq. (10) and for the numerical derivative of Eq. (11). Results are provided on Fig. 5. The histograms have been computed for the same parameter conditions as in Fig. 2, both for the same t_0 and Δt values for which Tracy-Widom (TW) and Baik-Rains (BR) distributions are obtained there for the KPZ equation. The histograms shown on Figs. 5(a),(b) are Gaussian to a high precision, compare the symbols in the figures with the exact Gaussian forms (solid lines). Also, the skewness and kurtosis shown on Figs. 5(c) and 5(d), respectively, are seen to readily take on their Gaussian (zero) values. All these results support the interpretation of the noisy Burgers equation as the derivative of the KPZ equation, as well as the Gaussian behavior of its fluctuations both, prior and after saturation to steady state, as assessed by our numerical simulations.

Asymmetric profiles

Also similar to the discussion provided above (see Fig. 3 there), and in analogy with the simulations provided in Figs. 4 and 5, we can assess the relevance of sawtooth-like features in the long-time behavior of the noisy Burgers equation, by evaluating the fluctuation histogram for the second-order space derivative (curvature field) of the KPZ equation. As expected, profiles are asymmetric for intermediate times within the nonlinear regime [Figs. 6(b)-(d)], away both from the linear [Figs. 6(a)] and saturation regimes [Figs. 6(e)], in which the surface is $x \leftrightarrow -x$. symmetric on average.

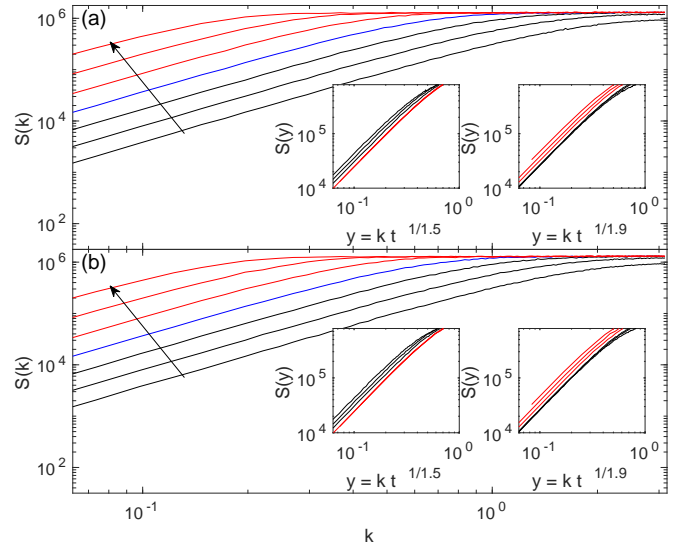


FIG. 4: Time evolution of the structure factor of solutions of the Burgers equation with conserved noise (a) and the slopes of the KPZ equation (b), for $D = 1$, $\lambda = 4$, $\nu = 1$ and $L = 256$. Black (red) solid lines correspond to the linear (nonlinear) regime, as implied by the collapse shown in the insets. Time increases following the arrow, t for each line being twice that of the previous one, starting at $t_0 = 0.64$. All units are arbitrary.

APPENDIX II: Dynamical Renormalization Group analysis of field statistics for the 1D noisy Burgers equation

This section provides some additional details on the evaluation of field cumulants for the noisy Burgers equation following the Dynamical Renormalization Group (DRG) approach of [44], previously applied to the evaluation of field statistics in the cases of the KPZ [39, 40, 42] and the non-linear Molecular Beam Epitaxy [41] equations, and of the Burgers equation with non-conserved noise [43].

According to Eq. (10), the n -th cumulant of u reads

$$\langle u^n \rangle_c = \int_{\mathbb{R}^{2(n-1)}} G(k_n, \omega_n) L_n \prod_{j=1}^{n-1} \frac{dk_j d\omega_j}{(2\pi)^2} G(k_j, \omega_j), \quad (12)$$

where $k_n = -\sum_{j=1}^{n-1} k_j$, $\omega_n = -\sum_{j=1}^{n-1} \omega_j$. The correction L_n is perturbatively computed to one loop order as

$$L_n = (2D)\delta_{n,2} + L_{n,1}, \quad (13)$$

where $L_{n,1} = K \lambda^n i^n k_n l_{n,1} \prod_{j=1}^{n-1} k_j$ is the lowest-order correction in the Feynman expansion of the cumulants, with $K = (2n-2)!!$ being a combinatorial factor (number of different fully-connected diagrams). As we are interested in the $(k_i, \omega_i) \rightarrow (0, 0)$ limit,

$$l_{n,1} = \int_{-\infty}^{\infty} \frac{d\Omega}{2\pi} \int_{-\infty}^{\infty} \frac{dq}{2\pi} |G_0(q, \Omega)|^{2n} (2Dq^2)^n, \quad (14)$$

where the integration domain in $\int_{-\infty}^{\infty}$ is the region $\{q \in$

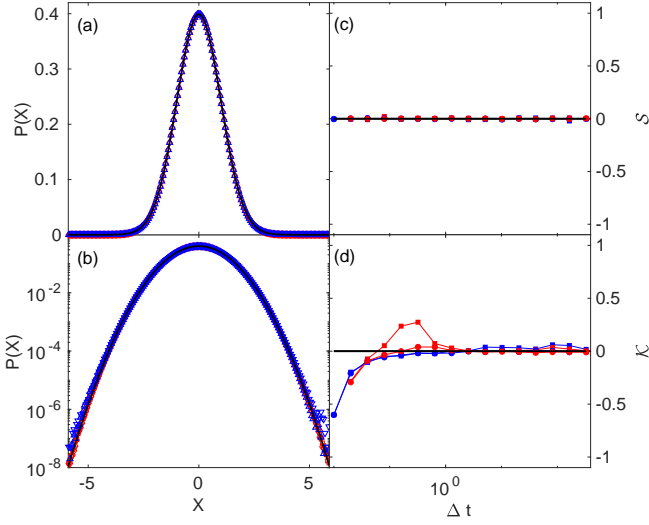


FIG. 5: Fluctuation [as defined in Eq. (4)] histogram for $t_0 = 0$ (blue) and $t_0 = t_{sat} = 300$ (red), and $\Delta t = 150$ from numerical simulations of Burgers equation with conserved noise (squares) and from the derivative (slope field) of numerical simulations of the KPZ equation (circles), using parameters as in Fig. 4(a),(b). The solid lines correspond to a Gaussian distribution. Time evolution of the fluctuations skewness (c) and kurtosis (d) for the same numerical simulations as in panels (a) and (b). All units are arbitrary.

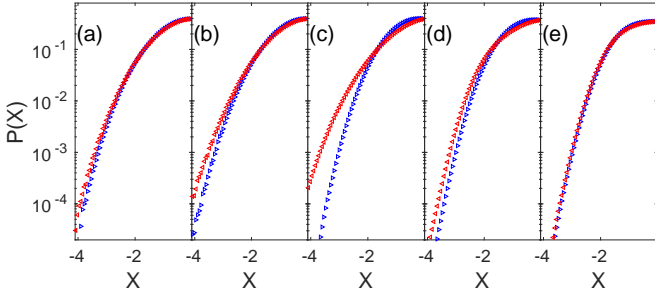


FIG. 6: Fluctuation histogram from numerical simulations of the curvature field (second-order space derivative) from numerical simulations of the KPZ equation, for times in the linear (a), nonlinear (b-d), and saturation (e) regimes (time for each panel is twice that of the previous one, starting at $t_0 = 40$). The histogram for $X > 0$ (red left triangles) has been reflected to facilitate comparison with the $X < 0$ (blue right triangles) data. Parameters as in Fig. 4, except for $\lambda = 10^4$ and $D = 10^{-3}$. All units are arbitrary.

$\mathbb{R}|\Lambda(\ell) = \Lambda_0 e^{-\ell} < |q| < \Lambda_0\}$. After integration,

$$l_{n,1} = \frac{2^{n+1}\Gamma(n - \frac{1}{2})}{4\pi^{3/2}(n-1)!} \frac{D^n \nu^{1-2n} e^{(3-2n)\ell} - 1}{\Lambda^{2n-3}(\ell) (3-2n)}. \quad (15)$$

Taking $\ell \rightarrow 0$, and considering the dependence of ν and D with Λ , [39], the following differential equation is obtained,

$$\frac{dl_{n,1}}{d\ell} = \frac{2^{n+1}\Gamma(n - \frac{1}{2})}{4\pi^{3/2}(n-1)!} \frac{(D\nu \frac{D\lambda^2}{2\pi\nu^3})^{(1-n)/4}}{\Lambda^{\frac{5}{2}(n-1)}(\ell)}, \quad (16)$$

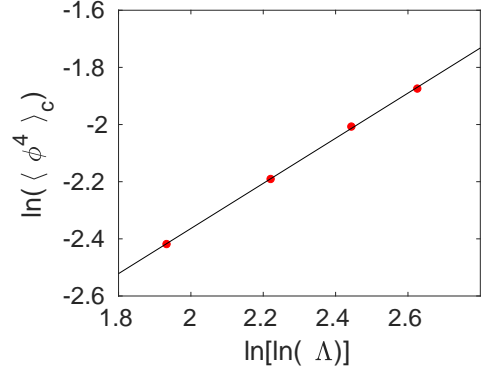


FIG. 7: Numerical computation of $\langle \phi^4 \rangle_c$ in the $[k_1, k_2, k_3] \in [1, \Lambda]^3$ region, for different values of Λ (symbols). The solid line shows a linear fit of the numerical data, and corresponds to the straight line $y = 0.79x - 3.94$, hence $\langle \phi^4 \rangle_c \sim (\ln \Lambda)^{0.79}$.

whose solutions for large ℓ become

$$l_{n,1}(\ell) \simeq \frac{2^{n+1}\Gamma(n - \frac{1}{2})}{4\pi^{3/2}(n-1)!} \frac{(D\nu \frac{D\lambda^2}{2\pi\nu^3})^{(1-n)/4}}{\frac{5}{2}(n-1)\Lambda^{\frac{5}{2}(n-1)}(\ell)}. \quad (17)$$

Due to symmetry among k_1, \dots, k_{n-1} , we take [39, 40, 42, 44]

$$l_{n,1}(k) = \frac{2^{n+1}\Gamma(n - \frac{1}{2})}{4\pi^{3/2}(n-1)!} \frac{(D\nu \frac{D\lambda^2}{2\pi\nu^3})^{(1-n)/4}}{\frac{5}{2}(n-1)} \prod_{j=1}^{n-1} \frac{1}{k_j^{5/2}}. \quad (18)$$

For $n > 1$, as $k^{5/2}f(\omega/k^z) = k^{-3/2}\nu(k)^{-2}|G(k, \omega)|^{-2}$, where f is a scaling function [$f(u) \rightarrow 1$ as $u \rightarrow 0$], we substitute $k_i^{-5/2} \simeq k_i^{3/2}\nu^2(k_i)|G(k_i, \omega_i)|^2$. Finally,

$$\langle u^n \rangle_c = A \int_{\mathbb{R}^{2(n-1)}} G(k_n, \omega_n) k_n \times$$

$$\prod_{i=1}^{n-1} \frac{dk_i d\omega_i}{(2\pi)^2} k_i G(k_i, \omega_i) k_i^{3/2} \nu^2(k_i) |G(k_i, \omega_i)|^2, \quad (19)$$

where $A = \pi^{n-1/2} i^n \Gamma(n-1/2) K 2D / [n!(n-1)\lambda^{n-2}]$.

APPENDIX III: Kurtosis behavior with lattice spacing

The fourth cumulant of the fluctuation distribution has been estimated for different values of the lattice spacing s by means of analytical integration in $\omega_1, \omega_2, \omega_3$, and numerical integration in k_1, k_2, k_3 . Parameters have been chosen so as to make $A = 1$ and $D\lambda^2/2\pi = 1$. Integration limits in k_1, k_2, k_3 of the form $[1, \Lambda]$ have been taken for different values of $\Lambda \propto 1/s$, in order to characterize the divergence of the integral with the lattice spacing s . The conclusion is that $\langle \phi^4 \rangle_c \sim (\ln \Lambda)^{0.79}$, see Fig. 7, a result which is employed after Eq. (7) above.

-
- * Electronic address: enrodrig@math.uc3m.es
† Electronic address: cuerno@math.uc3m.es
- [1] M. Kardar, G. Parisi, and Y.-C. Zhang, Dynamic Scaling of Growing Interfaces, *Phys. Rev. Lett.* **56**, 889 (1986).
 - [2] U. C. Täuber, *Critical Dynamics* (Cambridge University Press, Cambridge, England, 2014).
 - [3] R. Livi and P. Politi, *Nonequilibrium Statistical Physics: A Modern Perspective* (Cambridge University Press, Cambridge, England, 2017).
 - [4] W. Lenz, Beiträge zum Verständnis der magnetischen Eigenschaften in festen Körpern”, *Phys. Z.* **21**, 613 (1920).
 - [5] L. Onsager, Crystal Statistics. I. A Two-Dimensional Model with an Order-Disorder Transition, *Phys. Rev.* **65**, 117 (1944).
 - [6] T. Sasamoto and H. Spohn, One-Dimensional Kardar-Parisi-Zhang Equation: An Exact Solution and its Universality, *Phys. Rev. Lett.* **104**, 230602 (2010).
 - [7] G. Amir, I. Corwin, and J. Quastel, Probability Distribution of the Free Energy of the Continuum Directed Random Polymer in 1+1 Dimensions, *Commun. Pure Appl. Math.* **64**, 466 (2011).
 - [8] P. Calabrese and P. Le Doussal, Exact Solution for the Kardar-Parisi-Zhang Equation with Flat Initial Conditions, *Phys. Rev. Lett.* **106**, 250603 (2011).
 - [9] M. Henkel, *Conformal Invariance and Critical Phenomena* (Springer-Verlag, Berlin, 1999).
 - [10] For an overview on recent KPZ developments, see T. Halpin-Healy and K. A. Takeuchi, A KPZ Cocktail-Shaken, not Stirred..., *J. Stat. Phys.* **160**, 794 (2015).
 - [11] O. Hallatschek *et al.*, Genetic drift at expanding frontiers promotes gene segregation, *Proc. Natl. Acad. Sci. USA* **104**, 19926 (2007).
 - [12] K. A. Takeuchi *et al.*, Growing interfaces uncover universal fluctuations behind scale invariance, *Sci. Rep.* **1**, 34 (2011).
 - [13] H. van Beijeren, Exact results for anomalous transport in one-dimensional hamiltonian systems, *Phys. Rev. Lett.* **108**, 180601 (2012).
 - [14] C. B. Mendl and H. Spohn, Dynamic correlators of fermi-pastulam chains and nonlinear fluctuating hydrodynamics, *Phys. Rev. Lett.* **111**, 230601 (2013).
 - [15] P. J. Yunker *et al.*, Effects of Particle Shape on Growth Dynamics at Edges of Evaporating Drops of Colloidal Suspensions, *Phys. Rev. Lett.* **110**, 035501 (2013).
 - [16] R. A. L. Almeida, *et al.* Universal fluctuations in the growth of semiconductor thin films, *Phys. Rev. B* **89**, 045309 (2014).
 - [17] P. A. Orrillo, *et al.* Morphological stabilization and KPZ scaling by electrochemically induced co-deposition of nanostructured NiW alloy films, *Sci. Rep.* **7**, 17997 (2017).
 - [18] S. Nestic, R. Cuerno, and E. Moro, Macroscopic response to microscopic intrinsic noise in three-dimensional Fisher fronts, *Phys. Rev. Lett.* **113**, 180602 (2014).
 - [19] S. N. Santalla *et al.*, Random geometry and the Kardar-Parisi-Zhang universality class. *New J. Phys.* **17**, 33018 (2015).
 - [20] E. Altman, *et al.*, Two-dimensional superfluidity of exciton polaritons requires strong anisotropy, *Phys. Rev. X* **5**, 011017 (2015).
 - [21] L. Chen *et al.*, Mapping two-dimensional polar active fluids to two-dimensional soap and one-dimensional sandblasting, *Nature Comm.* **7**, 12215 (2016).
 - [22] A. Nahum *et al.*, Quantum entanglement growth under random unitary dynamics, *Phys. Rev. X* **7**, 031016 (2017).
 - [23] T. Kriecherbauer and J. Krug, A pedestrian’s view on interacting particle systems, KPZ universality and random matrices, *J. Phys. A: Math. Theor.* **43**, 403001 (2010).
 - [24] J.-Y. Fortin, and M. Clusel, Applications of Extreme Value Statistics, *J. Phys. A: Math. Theor.* **48**, 183001 (2015).
 - [25] D. Forster, D. R. Nelson, and M. J. Stephen, Large-distance and long-time properties of a randomly stirred fluid, *Phys. Rev. A* **16**, 732 (1977).
 - [26] G. Da Prato, A. Debussche, and R. Temam, Stochastic Burgers’ equation, *Nonlin. Diff. Eq. Appl.* **1**, 389 (1994).
 - [27] L. Bertini and G. Giacomin, Stochastic Burgers and KPZ Equations from Particle Systems, *Comm. Math. Phys.* **183**, 571 (1997).
 - [28] M. Gubinelli and M. Jara, Regularization by noise and stochastic Burgers equations, *Stoch. PDE Anal. Comp.* **1**, 325 (2013).
 - [29] U. Frisch, *Turbulence: the legacy of A. N. Kolmogorov* (Cambridge University Press, Cambridge, England, 1995).
 - [30] J. A. Krommes, Fundamental statistical descriptions of plasma turbulence in magnetic fields, *Phys. Rep.* **360**, 1 (2002).
 - [31] H. Spohn, *Large Scale Dynamics of Interacting Particles* (Springer-Verlag, Berlin, 1991).
 - [32] A.-L. Barabási and H. E. Stanley, *Fractal concepts in surface growth* (Cambridge University Press, Cambridge, England, 1995).
 - [33] J. Krug, Origins of scale invariance in growth processes, *Adv. Phys.* **46**, 139 (1997).
 - [34] K. Ueno, H. Sakaguchi, and M. Okamura, Renormalization-group and numerical analysis of a noisy Kuramoto-Sivashinsky equation in 1+1 dimensions, *Phys. Rev. E* **71**, 046138 (2005).
 - [35] M. Hairer and J. Voss, Approximations to the Stochastic Burgers Equation, *J. Nonlinear. Sci.* **21**, 897 (2011).
 - [36] T. Sasamoto and H. Spohn, Superdiffusivity of the 1D lattice Kardar-Parisi-Zhang equation, *J. Stat. Phys.* **137**, 917 (2009).
 - [37] K. A. Takeuchi, Crossover from Growing to Stationary Interfaces in the Kardar-Parisi-Zhang Class, *Phys. Rev. Lett.* **110**, 210604 (2013).
 - [38] D. Squizzato, L. Canet, and A. Minguzzi, Kardar-Parisi-Zhang universality in the phase distributions of one-dimensional exciton-polaritons, *Phys. Rev. B* **97**, 195453 (2018).
 - [39] T. Singha and M. K. Nandy, Skewness in (1 + 1)-dimensional Kardar-Parisi-Zhang-type growth, *Phys. Rev. E* **90**, 062402 (2014).
 - [40] T. Singha and M. K. Nandy, Kurtosis of height fluctuations in (1 + 1) dimensional KPZ Dynamics, *J. Stat. Mech.: Theor. Exp.* (2015), 05020.
 - [41] T. Singha and M. K. Nandy, Hyperskewness of (1+1)-dimensional KPZ height fluctuations, *J. Stat. Mech.: Theor. Exp.* (2016), 013203.
 - [42] T. Singha and M. K. Nandy, A renormalization scheme and skewness of height fluctuations in (1 + 1)-dimensional VLDS dynamics, *J. Stat. Mech.: Theor. Exp.* 023205 (2016).
 - [43] E. Rodriguez-Fernandez and R. Cuerno, Gaussian statistics as an emergent symmetry of the stochastic scalar Burgers equation, *Phys. Rev. E* **99**, 042108 (2019).
 - [44] V. Yakhot and S. A. Orszag, Renormalization-Group Analysis of Turbulence, *Phys. Rev. Lett.* **57**, 1722 (1986).
 - [45] I. S. S. Carrasco and T. J. Oliveira, Universality and geometry dependence in the class of the nonlinear molecular beam epitaxy equation, *Phys. Rev. E* **94**, 050801(R) (2016).
 - [46] J. M. Burgers, *The Nonlinear Diffusion Equation* (D. Reidel, Dordrecht, Holland, 1974).
 - [47] S. Bendaas, Periodic wave shock solutions of Burgers equations, *Cogent Math. Stat.* **5**, 1463597 (2018).
 - [48] For a study of Eq. (3) with step boundary conditions, see H. Sakaguchi, Shock Structures and Velocity Fluctuations in the Noisy Burgers and KdV-Burgers Equations, *Prog. Theor. Phys.*

- 110**, 187 (2003).
- [49] E. Vivo, M. Nicoli, and R. Cuerno, Strong anisotropy in two-dimensional surfaces with generic scale invariance: Gaussian and related models, *Phys. Rev. E* **86**, 051611 (2012).
- [50] E. Vivo, M. Nicoli, and R. Cuerno, Strong anisotropy in two-dimensional surfaces with generic scale invariance: Nonlinear effects, *Phys. Rev. E* **89**, 042407 (2014).
- [51] T. Hwa and M. Kardar, Avalanches, hydrodynamics, and discharge events in models of sandpiles, *Phys. Rev. A* **45**, 7002 (1992).